Geomechanics and Engineering, *Vol. 27, No. 5 (2021) 433-445*
https://doi.org/10.12989/gae.2021.27.5.433

Experimental and numerical investigation of closure time during artificial ground freezing with vertical flow

Hyunwoo Jin[1], Gyu-Hyun Go[2], Byung Hyun Ryu[1] and Jangguen Lee*[1]

[1]*Department of Future and Smart Construction Research, KICT, 283, Goyang daero, Ilsanseo gu, Goyang si, Gyeonggi do, Republic of Korea*
[2]*Department of Civil Engineering, Kumoh National Institute of Tech., 61, Daehak-ro, Gumi-si, Gyeongsangbuk-do, Republic of Korea*

(Received July 7, 2021, Revised November 21, 2021, Accepted November 22, 2021)

Abstract. Artificial ground freezing (AGF) is a commonly used geotechnical support technique that can be applied in any soil type and has low environmental impact. Experimental and numerical investigations have been conducted to optimize AGF for application in diverse scenarios. Precise simulation of groundwater flow is crucial to improving the reliability these investigations' results. Previous experimental research has mostly considered horizontal seepage flow, which does not allow accurate calculation of the groundwater flow velocity due to spatial variation of the piezometric head. This study adopted vertical seepage flow-which can maintain a constant cross-sectional area-to eliminate the limitations of using horizontal seepage flow. The closure time is a measure of the time taken for an impermeable layer to begin to form, this being the time for a frozen soil-ice wall to start forming adjacent to the freeze pipes; this is of great importance to applied AGF. This study reports verification of the reliability of our experimental apparatus and measurement system using only water, because temperature data could be measured while freezing was observed visually. Subsequent experimental AFG tests with saturated sandy soil were also performed. From the experimental results, a method of estimating closure time is proposed using the inflection point in the thermal conductivity difference between pore water and pore ice. It is expected that this estimation method will be highly applicable in the field. A further parametric study assessed factors influencing the closure time using a two-dimensional coupled thermo-hydraulic numerical analysis model that can simulate the AGF of saturated sandy soil considering groundwater flow. It shows that the closure time is affected by factors such as hydraulic gradient, unfrozen permeability, particle thermal conductivity, and freezing temperature. Among these factors, changes in the unfrozen permeability and particle thermal conductivity have less effect on the formation of frozen soil–ice walls when the freezing temperature is sufficiently low.

Keywords: artificial ground freezing; closure time; groundwater; model test; parametric study; vertical flow

1. Introduction

Soil improvement using geotextiles, preloading, grouting, and artificial ground freezing (AGF), among other methods, has attracted considerable research attention (Tandel *et al.* 2014, Quang and Giao, 2014, Chang *et al.* 2016, Taha *et al.* 2018). One of the most commonly used techniques for ground support is AGF, which circulates a refrigerant such as brine or injects liquefied gas such as liquid nitrogen in a freeze pipe buried in the ground to form an impermeable zone (Marwan *et al.* 2016, Huang *et al.* 2018). This technique can solve geotechnical engineering problems including groundwater control and excavation support during underground construction while having low environmental impact (Jessberger 1980, Andersland and Ladanyi, 2004, Jin *et al.* 2020). In comparison with other geotechnical support methods, AGF is not limited to a specific soil type (Alzoubi *et al.* 2020) and can be used in fine-grained soil such as silt and clayey sand (Zhou and Tang, 2018) or fractured sedimentary rocks such as sandstone (Shen *et al*. 2018).

*Corresponding author, Ph.D.
E-mail: jlee@kict.re.kr

Over the last few decades, several fundamental studies have investigated AGF with respect to the influence of factors such as freeze pipe diameter, pipe spacing, pipe orientation, refrigerant temperature, and groundwater flow (Pimentel *et al.* 2012, Alzoubi *et al.* 2019). These studies ultimately aimed to optimize the field applicability of AGF in diverse scenarios (Alzoubi *et al.* 2020). To study the efficiency of AGF with respect to various influencing factors, the groundwater flow must first be taken into account (Hashemi and Sliepcevich 1973, Frivik and Comini 1982, Lackner *et al.* 2005, Pimentel *et al.* 2012a, 2012b, Zhou and Meschke, 2013, Yu *et al.* 2014, Vitel *et al.* 2016b, Shin *et al.* 2018, Alzoubi *et al.* 2019, Wang *et al.* 2019, Li *et al.* 2019). Several laboratory-scale AGF experimental studies have therefore considered groundwater flow. Most experimental studies (Frivik and Comini 1982, Pimentel *et al.* 2012b, Alzoubi *et al.* 2018, Wang *et al.* 2019, Zueter *et al.* 2020) simulated groundwater flow horizontally. However, Fig. 1(a) shows it is difficult to control the piezometric head due to unconfined two-dimensional flow. The groundwater flow velocity cannot be accurately estimated because the cross-sectional area is not controlled. In contrast, Fig. 1(b) shows that using vertical flow allows simulation of a complete confined flow with constant cross-section and thus precise estimation of flow velocity. Ständer (1967) introduced laboratory AGF tests with vertical flow in

ISSN: 2005-307X (Print), 2092-6219 (Online)

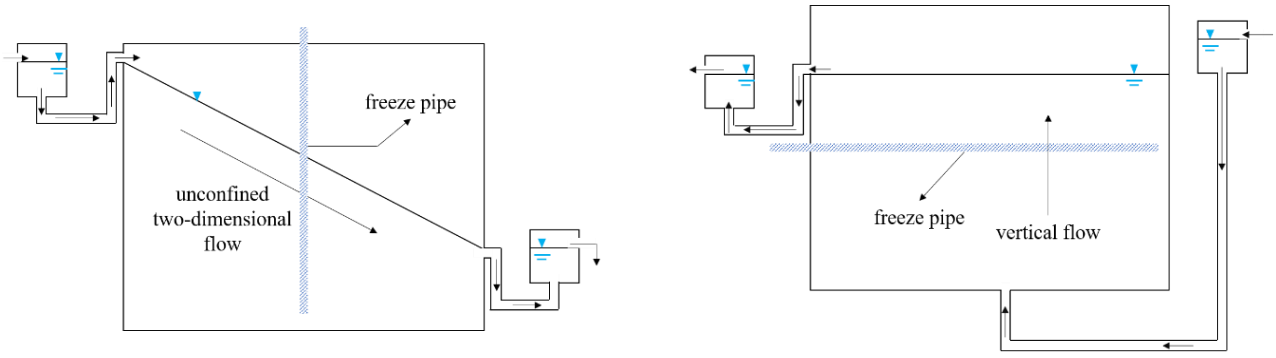

(a) horizontal flow (b) vertical flow

Fig. 1 Flow direction effect in the AGF model test

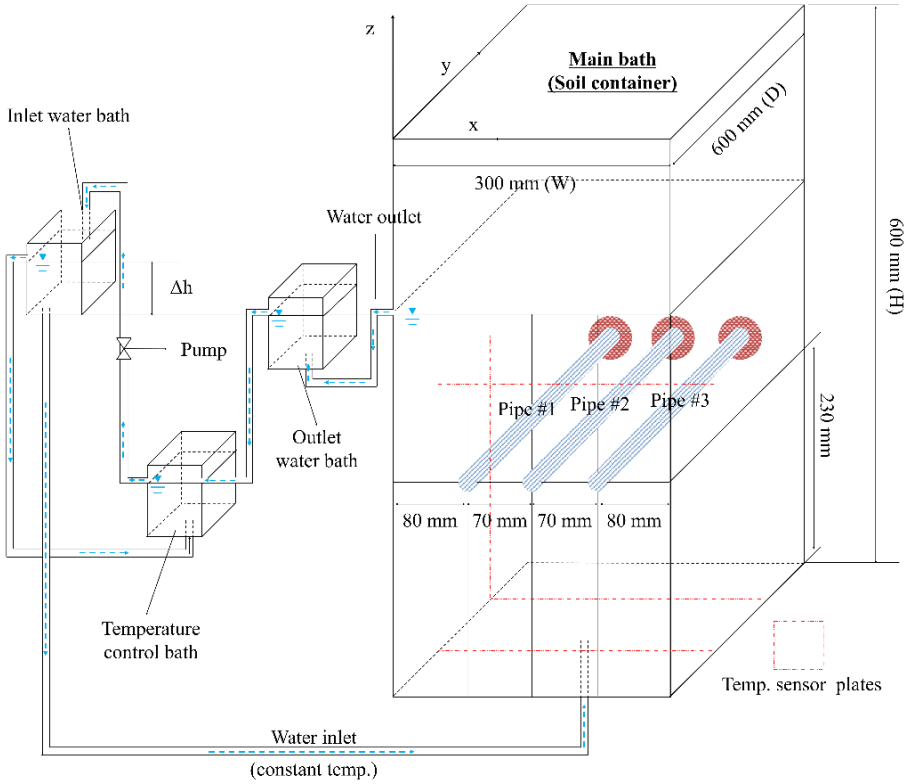

(a) closed-loop circulation system for AGF laboratory test

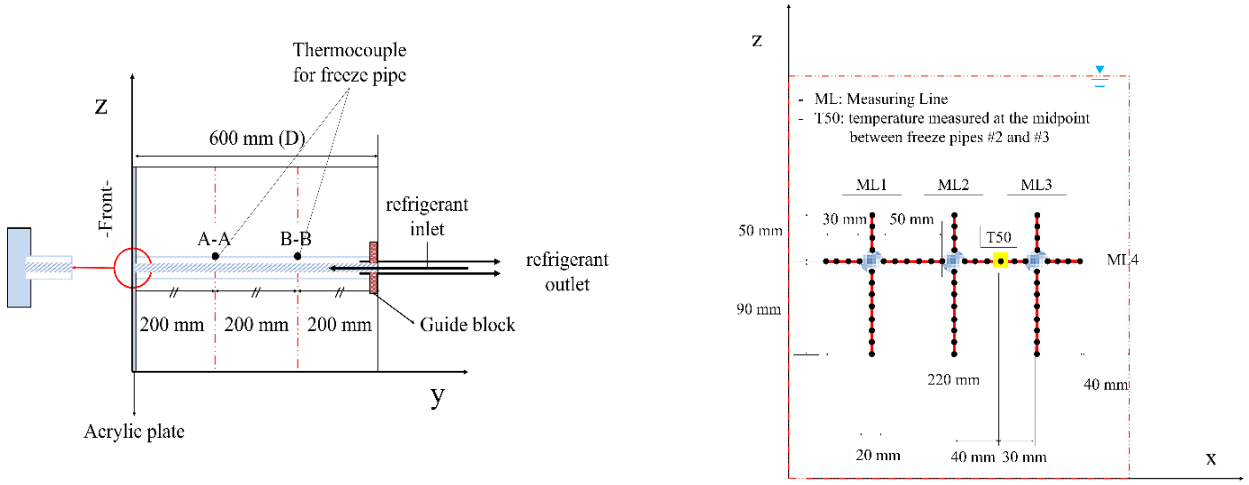

(b) longitudinal section (c) cross section of temperature sensor plate

Fig. 2 Schematic diagram of laboratory-scale AGF testing equipment (Jin *et al.* 2020)

Table 1 Summary of experimental conditions for AGF

Material	Flow direction	Temp. (°C)		Dry unit weight (g/cm^3)	Porosity	Flow (discharge) rate (m^3/s)	Flow velocity (m/d)
		Initial (meas.)	Freeze pipe (setting)				
Water	Vertical (bottom → top)	4	−10	-	-	-	-
		5				3.33×10^{-6}	1.60
Saturated sandy soil		10				-	-
		10		1.50	0.44	2.40×10^{-6}	1.15
		10				4.58×10^{-6}	2.20

medium sand, but the flow was stopped after the initial temperature reached a specified value, and so did not conduct a laboratory AGF test with vertical flow. Experimental data are generally insufficient to evaluate numerical results and determine closure time, which is defined as the time taken for the freezing around adjacent freeze pipes to merge. Although the closure time is the most important parameter determining AGF efficiency, it has not yet been studied in detail.

This paper reports a new closed-loop AGF laboratory testing system with vertical seepage flow. The system's 118 sensors measured temporal and spatial temperature data: 56 thermocouples, one for each temperature sensor plate, were installed around three freeze pipes, and two more thermocouples were attached to each freeze pipe. The three horizontal freeze pipes were perpendicular to the flow direction. Testing the experimental model used only water so that the freezing could be visually observed; closure times were measured with and without water flow. After verification of the experimental model, AGF tests used fully saturated sandy soil. The experimental results with only water and saturated sandy soil were compared, and a simple method for estimating closure time was proposed. A coupled thermal–hydraulic numerical analysis model was verified by comparing measured and calculated temperature results, and a further parametric study more deeply explored factors influencing closure time.

2. Testing equipment and program

2.1 Closed-loop AGF laboratory testing model

The new closed-loop AGF testing equipment for simulating vertical groundwater flow with two temperature sensor plates and three freeze pipes is illustrated in Fig. 2. The acrylic transparent soil container (300, 600, and 600 mm along the x-, y-, and z-axis, respectively) is fully insulated with 20 mm insulator (eXtruded Poly Styrene, XPS). Temperature-controlled water is pumped into a bottom inlet water bath (Fig. 2(a)). Water is supplied from the bottom, and the flow rate is controlled by the total head difference (Δh). Three double ring-shaped freeze pipes (API-5L-X42, 20 mm diameter) are installed horizontally in the soil container, perpendicular to the vertical flow direction shown in Fig. 2(b). Each double ring-shaped freeze pipe has an attached cooling pump. Refrigerant enters the inner ring and comes out of the outer ring. To maintain the horizontal level of each freeze pipe, one end is fixed with a guide block and the other is fixed by inserting the pipe into holes on the acrylic surface of the soil container. Two thermocouples and two temperature sensor plates are attached to each freeze pipe and installed at 200 mm intervals in the y-direction to measure the temperature variation during AGF laboratory tests (Fig. 2(b)). Fig. 2(c) depicts the arrangement of the cross-sectional temperature sensor plate. There are 12 temperature sensors (±0.5℃ accuracy), four above and eight below each freeze pipe at 10 mm intervals on a vertical line for each pipe. A further 20 temperature sensors are installed at 10 mm intervals along the horizontal center line of the three freeze pipes.

2.2 Laboratory testing conditions

Laboratory tests used water and fully saturated sandy soil ($\underline{D_{50}}$ = 0.47 mm). The seepage flow direction was controlled vertically from the bottom upward. Table 1 gives that the initial temperature for water-only testing was controlled at ~4℃ to minimize natural convection induced by temperature-dependent density differences. The tests were conducted with either no flow or a flow velocity of 1.60 m/d.

Tests with fully saturated sand had the initial temperatures controlled at ~10℃, a representative underground temperature. The sand's dry unit weight and porosity were 1.5 g/cm^3 and 0.44, respectively. The tests were conducted under three flow velocity conditions (no flow, 1.15 m/d, and 2.20 m/d). The temperature boundary conditions around the freeze pipes and at the bottom inlets are shown in Fig. 3.

3. Numerical modeling

3.1 Mass-balance equation

This study simulated the freezing of saturated sandy soil by regarding the soil as a three-phase structure consisting of soil particles, water, and ice. The mass-conservation equation is

$$\frac{d}{dt}(\rho_i \theta_i) + \frac{d}{dt}(\rho_w \theta_w) + \rho_w \nabla q = 0 \quad (1)$$

where t is time, θ_i and θ_w are the volumetric content of ice and pore water, respectively; ρ_i and ρ_w are their

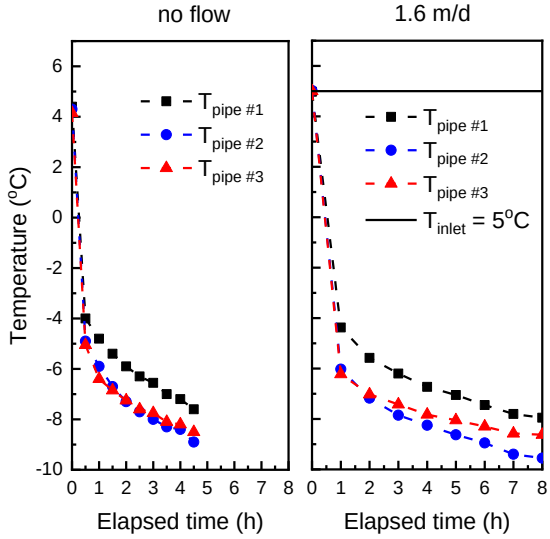

(a) only water

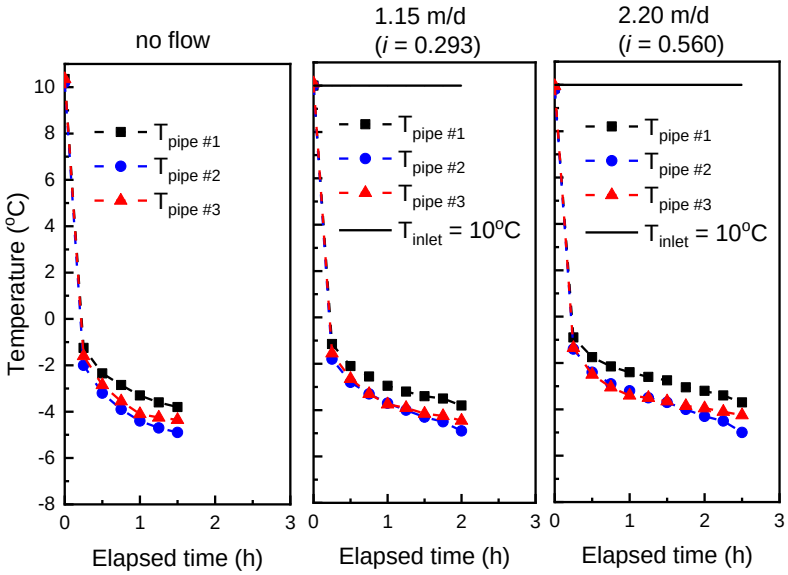

i = hydraulic gradient

(b) saturated sand

Fig. 3 Progression of temperature measured at freeze pipes and bottom lines for different flow rates

respective densities (kg/m^3). The groundwater velocity in the unfrozen area q is calculated by Eq. (2).

$$q = -k_r \frac{k_{uf}}{\mu} \nabla p \tag{2}$$

$$k_r(\theta_w) = \sqrt{\frac{\theta_w}{n}} \left(1 - \left(1 - \left(\frac{\theta_w}{n}\right)^{1/m}\right)^m\right)^2 \tag{3}$$

where p is the pore water pressure (Pa); k_{uf} is the initial intrinsic permeability in the unfrozen zone. The unitless relative permeability k_r is a function of the temperature-dependent volumetric contents (Luckner *et al.* 1989).

3.2 Energy-balance equation

The following energy-conservation equation was used to estimate the temperature change of the ground due to pipe freezing (Coussy 2004, Michalowski and Zhu 2006).

$$C \frac{\partial T}{\partial t} - L \frac{\partial \theta_i}{\partial t} \rho_i + \nabla(-\lambda \nabla T) + \rho_w C_w q \nabla T = 0 \tag{4}$$

where T is temperature (K), and L is the latent heat of fusion (L = 334.5 kJ/kg). This equation has a term indicating energy release due to the phase change of pore water during freezing added to the Fourier equation; the effective heat capacity C and effective soil thermal conductivity λ varied with temperature:

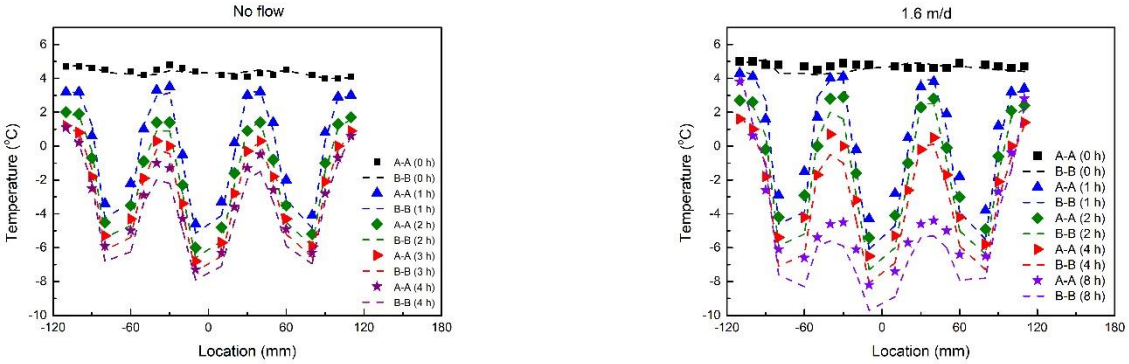

(a) horizontal orientation temperature measurement data with elapsed time (A-A & B-B)

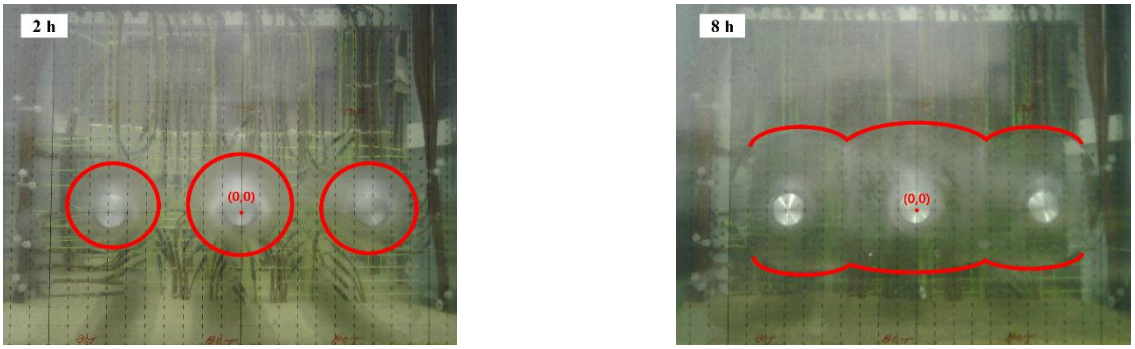

(b) ice column and wall shape under a flow of 1.6 m/d (Jin *et al.* 2020)

Fig. 4 Temperature plots and photographs during freezing

$$C = (1-n)\rho_s C_s + \theta_w \rho_w C_w + \theta_i \rho_i C_i \quad (5)$$

$$\lambda = {\lambda_s}^{\theta_s}\ {\lambda_w}^{\theta_w}\ {\lambda_i}^{\theta_i} \quad (6)$$

where n is porosity; the subscripts s, w, and i denote soil particles, pore water, and ice, respectively.

4. Experimental results

4.1 Experimental verification with only water

Artificial freezing tests were conducted with only water to verify the reliability of the equipment. This had the advantage of allowing the ice expansion shape to be visually observed. Vertical temperature distributions for each pipe were obtained from the two temperature sensor plates, and were named ML1, ML2, and ML3 for each pipe; a horizontal temperature distribution was named ML4 (see Fig. 2(c)). Temperatures measured by the two temperature sensor plates A-A and B-B at ML4 with and without vertical water flow are shown in Fig. 4(a). The longitudinal temperature distributions around the freeze pipes decreased at a similar freezing rate. The ice visibly expanded around each freeze pipe (see Fig. 4(b)) and kept a constant thickness in the longitudinal direction. The measured temperature data and visual investigation of the ice wall formation indicated that the conditions of the freeze pipes and the vertical flow were well controlled. Longitudinal temperature variation was negligible, obviating the need to present experimental results from both temperature sensor plates. Therefore, average temperature data from the two sensor plates are discussed.

The average vertical temperature distributions at ML1, ML2, and ML3 in Fig. 5 show that even though water did not flow and the temperature sensors were vertically located at the same distance along the freeze pipe, an asymmetric temperature distribution developed along each freeze pipe. This was due to natural convection caused by density differences that occurred during freezing. Temperatures measured above the freeze pipes were slightly higher under the flow condition than with no flow, and temperatures below the freeze pipes converged rapidly to 5°C when there was flow. Ice expansion progressed in an increasingly sized oval shape in a direction opposite to the water flow (Jumikis 1979, Jin *et al.* 2020). The bottom inlet boundary maintained a constant temperature, and the top outlet boundary clearly showed no heat flux.

As shown in Fig. 4, an ice wall was formed when the temperature between adjacent freeze pipes at ML4 was around −1°C, as confirmed by visual observation. That is, temperatures at 4 h and 5.5 h at the onset of the ice wall formation for no flow and a flow of 1.6 m/d, respectively, are shown in Fig. 6. Asymmetric temperature distributions again developed along each freeze pipe at the closure time (Fig. 6(a)–(c)): the asymmetric distribution was clear in the flow condition and resulted from the continuous thermal energy supply of the 5°C water. Temperatures at ML2 were slightly lower than those at ML1 and ML3. Similarly, temperatures at ML4 were slightly lower around freeze pipe #2 than the other two pipes. This is reasonable as the central pipe's cooling is aided by the others, in line with previous

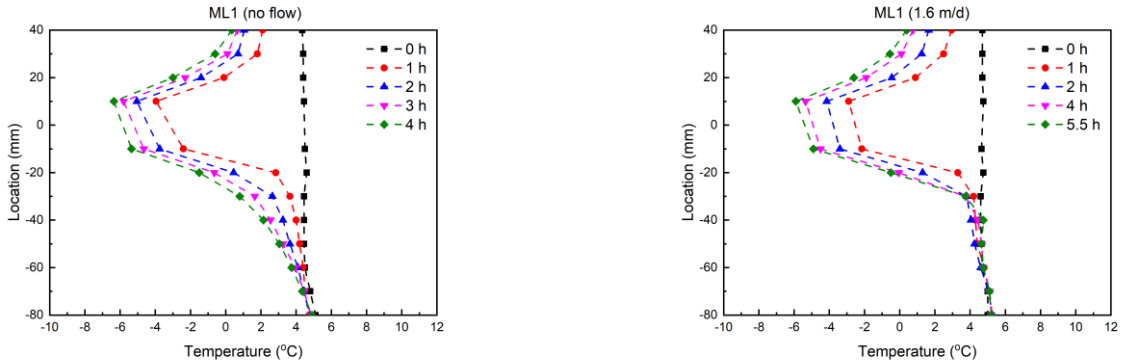

(a) ML1

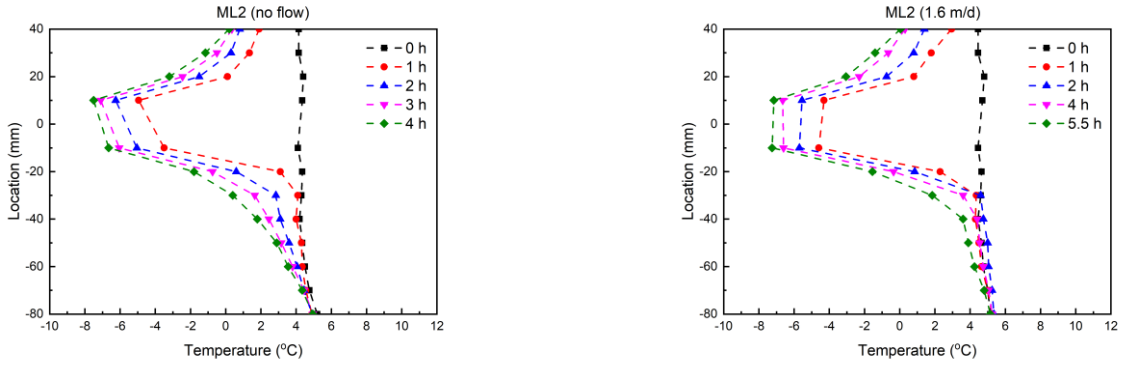

(b) ML2

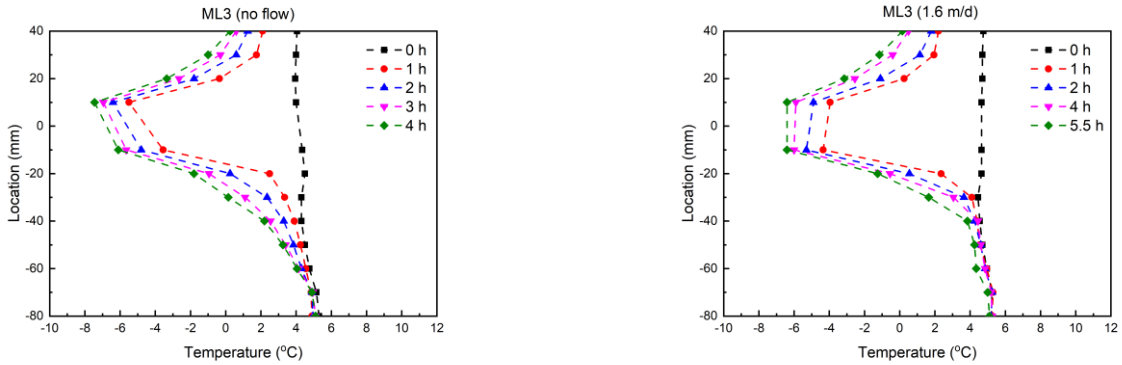

(c) ML3

No flow 1.6 m/d

Fig. 5 Measured vertical temperature distribution with elapsed time

studies finding that ice around the central freeze pipe expands a little more quickly and becomes slightly larger due to the effect of the neighboring pipes (Takashi 1969, Jumikis 1979). Interestingly, the temperature distributions at ML4 between the freeze pipes immediately after ice wall formation (i.e., at closure time) were largely the same regardless of the flow condition (Fig. 6(d)). As the ice wall prevents water flow after the closure time, the temperature distribution inside the ice wall is expected to be similar in both flow conditions. However, temperatures near both side boundaries at closure time were higher with flow than without. As the ice wall blocks water flow and flow velocity increases near both side boundaries, thermal convection increases, reducing the cooling effect of the freeze pipes. The measured temperature profiles and boundary conditions show that this closed-loop AGF system is well controlled and thus can potentially provide reliable experimental data when groundwater flow is simulated.

4.2 Laboratory AGF tests

The AGF tests using saturated sandy soil considered three flow conditions. After the initial temperature condition was set by sufficiently circulating water at 10℃, freezing tests were conducted by circulating a refrigerant at −10℃ under flow conditions of 0, 1.15, and 2.20 m/d. Fig. 7 shows average temperatures at ML4 with elapsed time. Similar to the testing results with only water, the

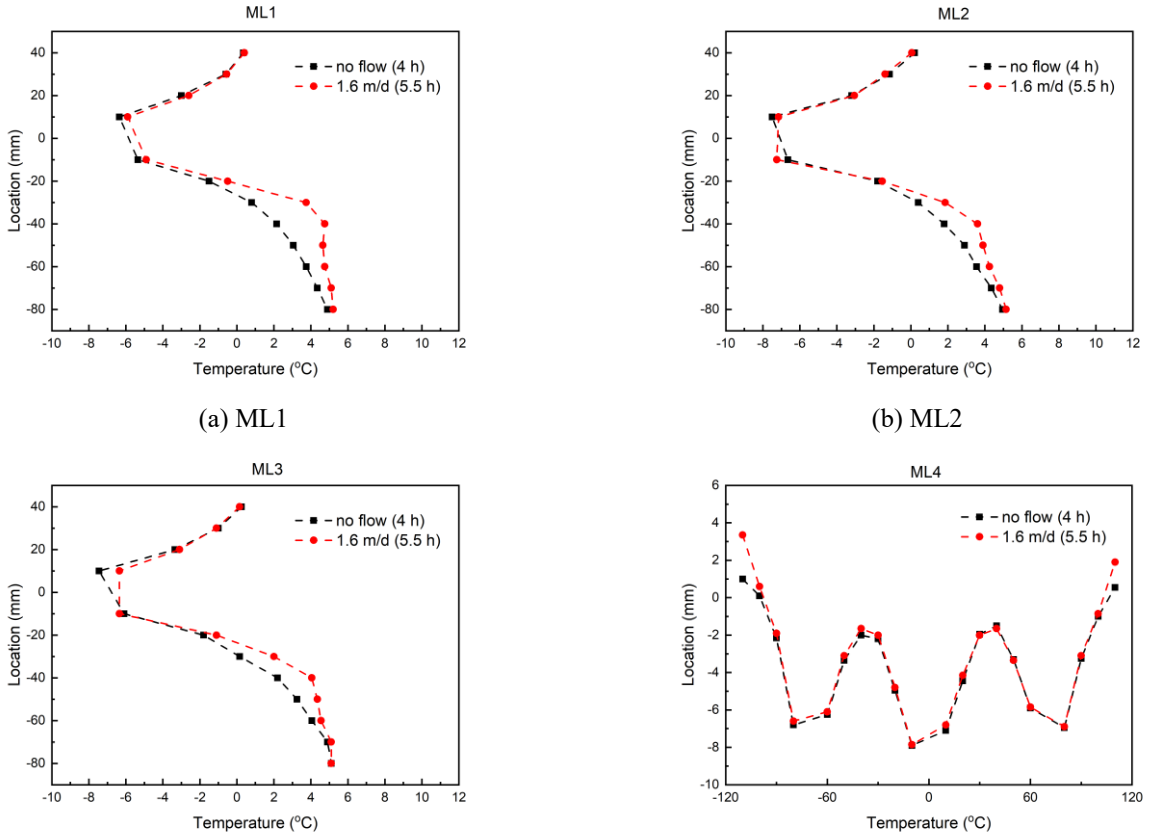

Fig. 6 Temperature measurement data at closure time

temperatures measured near the central freeze pipe decreased more quickly than elsewhere, but the difference was insignificant. The estimated closure times for flows of 0, 1.15, and 2.20 m/d were 1–1.5, 1.5–2, and 2–2.5 h, respectively.

Measured temperatures at ML1, ML2, ML3, and ML4 at each closure time under the three flow conditions are shown in Fig. 8. Under no flow, vertical temperature distributions were symmetric along the freeze pipes, strongly suggesting that the asymmetric temperature distribution seen with only water was caused by variation of the water density with changing temperature (see Fig. 6(a)–(c)). The flowing 10°C water, a continuously supplied source of thermal energy, resulted in asymmetric temperature distributions along the freeze pipes. Temperatures at ML4, especially between the freeze pipes, were almost the same at closure time regardless of the flow condition, which was observed with only water (see Fig. 6(d)). Temperatures near both side boundaries at closure time increased as the flow velocity increased, confirming the consistency of the results.

4.3 Numerical model verifiaction

Although the testing equipment was three dimensional (Fig. 2), there was no significant difference in the observation results in the longitudinal direction (i.e., along the y-axis); therefore, numerical simulation was in two dimensions. To simulate groundwater flow, a constant head difference (Δh) was maintained between the top and bottom. Temperatures measured on the three experimental freeze pipes were used as a Dirichlet boundary condition at the outer wall of the freeze pipe in the numerical model. The bottom boundary of the domain was maintained at 10°C, this being the initial temperature. Thermally insulated conditions were applied to the walls and the top of the domain. A commercial code (the COMSOL Multiphysics

Table 2 Material properties for numerical simulation

Property	Symbol	Value	Unit
Porosity	n	0.44	
Unfrozen permeability	k_{uf}	8.5×10^{-12}	m^2
Density of water	ρ_w	1000	kg/m^3
Density of ice	ρ_i	917	kg/m^3
Density of solid	ρ_s	2664	kg/m^3
Heat capacity of water	C_w	4200	J/(kg·K)
Heat capacity of ice	C_i	2100	J/(kg·K)
Heat capacity of solid	C_s	826	J/(kg·K)
Thermal conductivity of water	λ_w	0.6	W/(m·K)
Thermal conductivity of ice	λ_i	2.3	W/(m·K)
Thermal conductivity of solid	λ_s	6.2	W/(m·K)
Latent heat of fusion	L	3.33×10^5	J/kg

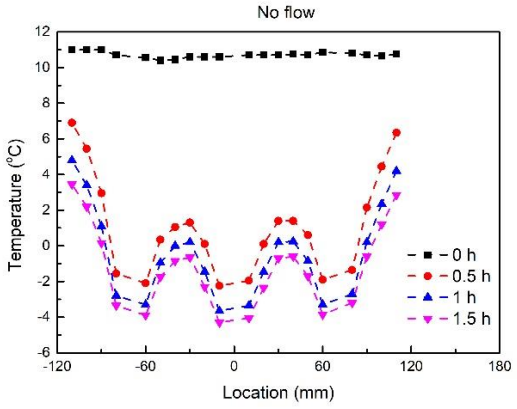

(a) no flow

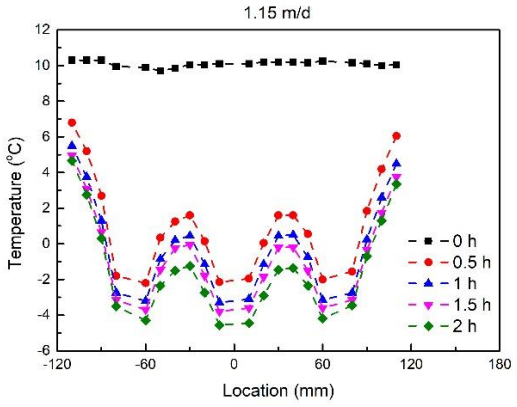

(b) 1.15 m/d

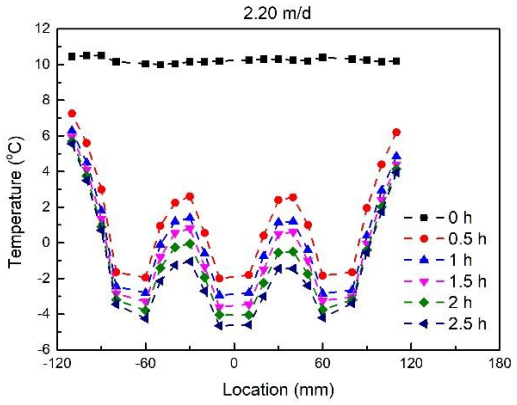

(c) 2.20 m/d

Fig. 7 Average measured temperature data with elapsed time at ML4

PDE module) applied the aforementioned constitutive equations in chapter 3 and boundary conditions (Comsol Inc. 2021). The analysis used 6758 triangular meshes. Table 2 lists the material properties used in the model.

Fig. 9 shows numerical results for two different hydraulic gradient conditions (i = 0.293, 0.560). Based on the ice content and temperature distribution, the closure times were estimated to be 1.88 and 2.42 h, respectively. The numerically estimated closure times are very similar to the observed values of 1.5–2 h for 1.15 m/d and 2–2.5 h for 2.20 m/d. Figures 10 and 11 give temperature distributions at ML1, ML2, ML3, and ML4 at closure time. The numerical model reasonably estimated the measured temperature data. In particular, the simulated temperature for ML4, which is important for the accurate estimation of closure time, well matched the observation.

5. Discussion: closure time estimation

Research on the time at which an impermeable layer starts to form (i.e., the closure time) and the factors affecting the formation of a frozen soil–ice wall is of great importance to the efficient application of AGF. The formation of a frozen soil–ice wall in geotechnical engineering cannot be visually observed, and sensor installation is limited in the field. Therefore, indirect methods to estimate the closure time considering cost and efficiency would be helpful.

Fig. 12 shows the temperature measured at the midpoint between freeze pipes #2 and #3 (T50, see Fig. 2(c)) during the freezing of saturated sandy soil. The inflection points of T50 appeared in a semi-logarithmic plot at the same time as the closure time previously obtained from the temperature data. The temperature drop accelerated at this point, because the thermal conductivity increased as pore water was replaced by ice as the frozen soil–ice wall formed. Therefore, the slope before and after the inflection point will differ depending on the ground's thermal conductivity. Based on these results, when AGF stabilizes ground where visual observation is not possible, the closure time could be estimated indirectly using the temporal midpoint temperature data between adjacent freeze pipes.

6. Parametric study

A parametric study explored the factors influencing the formation of frozen soil–ice walls. The closure time is redefined here as the time when the relative permeability coefficient (k_r) between adjacent freeze pipes (at T50) decreased to less than 1/100 of its initial value. Fig. 13 shows that at T50 it does not decrease when the hydraulic gradient (i) is higher than the critical hydraulic gradient (i_{cr}). Figure 14 shows that the closure time increases as i increases. When the flow velocity increases beyond the critical value, it is difficult to operate the AGF system until the closure time is reached. Therefore, i and the unfrozen permeability (k_{uf}) appear to be the key factors influencing the hydraulic behavior.

Additional important factors influencing the thermal behavior are the thermal conductivity of solid particles (λ_s) and the cooling temperature of the freeze pipe. The former affects the expansion rate of the frozen pillar during freezing (Go *et al.* 2020). The temperature difference between the freeze pipe and the ground determines the freezing rate. Therefore, parametric studies considered the parameters i, k_{uf}, λ_s, and the temperature of the freeze pipe. Table 4 lists reference unfrozen permeability ($k_{uf,ref}$) values calculated through comparison of flow velocity with test data at the same hydraulic head condition.

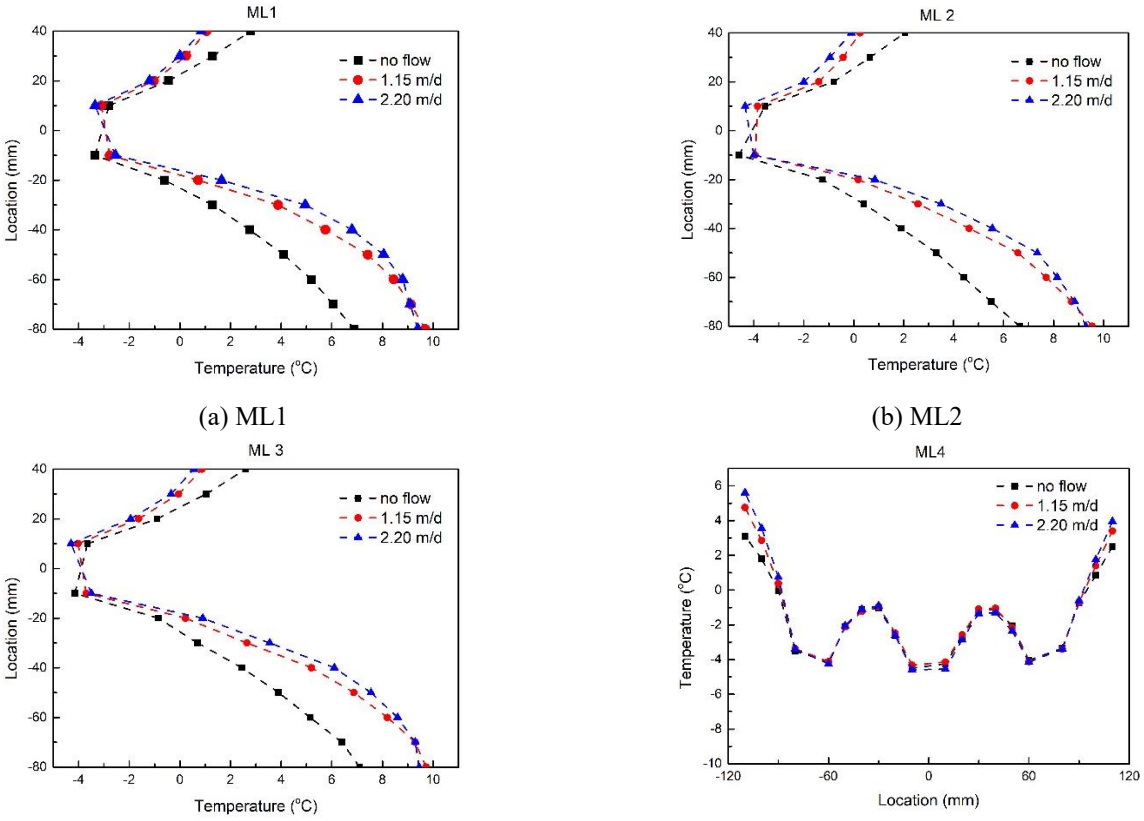

(a) ML1 (b) ML2

(c) ML3 (d) ML4

Fig. 8 Temperature measurement data at closure time

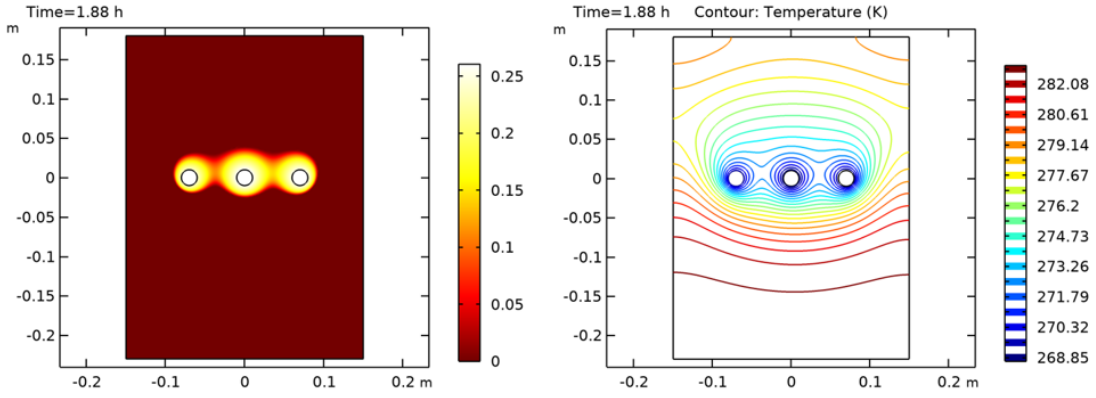

(a) ice content and temperature for i = 0.293

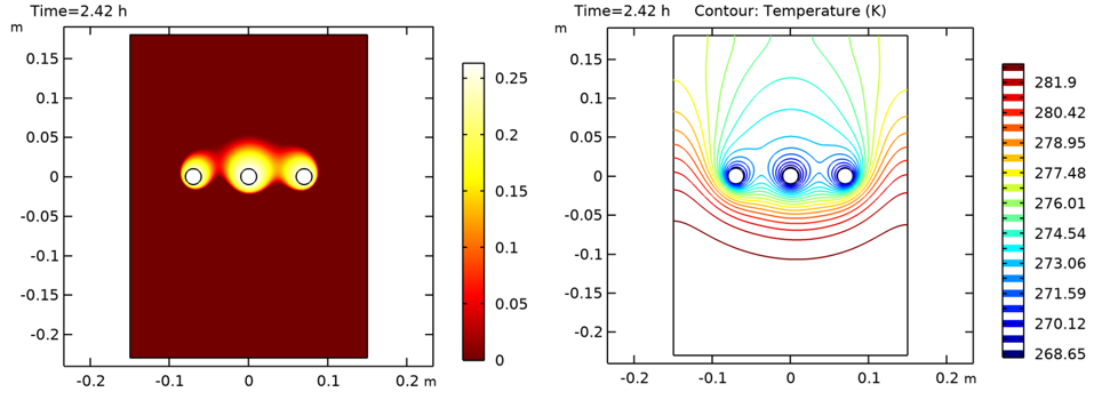

(b) ice content and temperature for i = 0.560

Fig. 9 Numerical analysis results for two different hydraulic gradient conditions

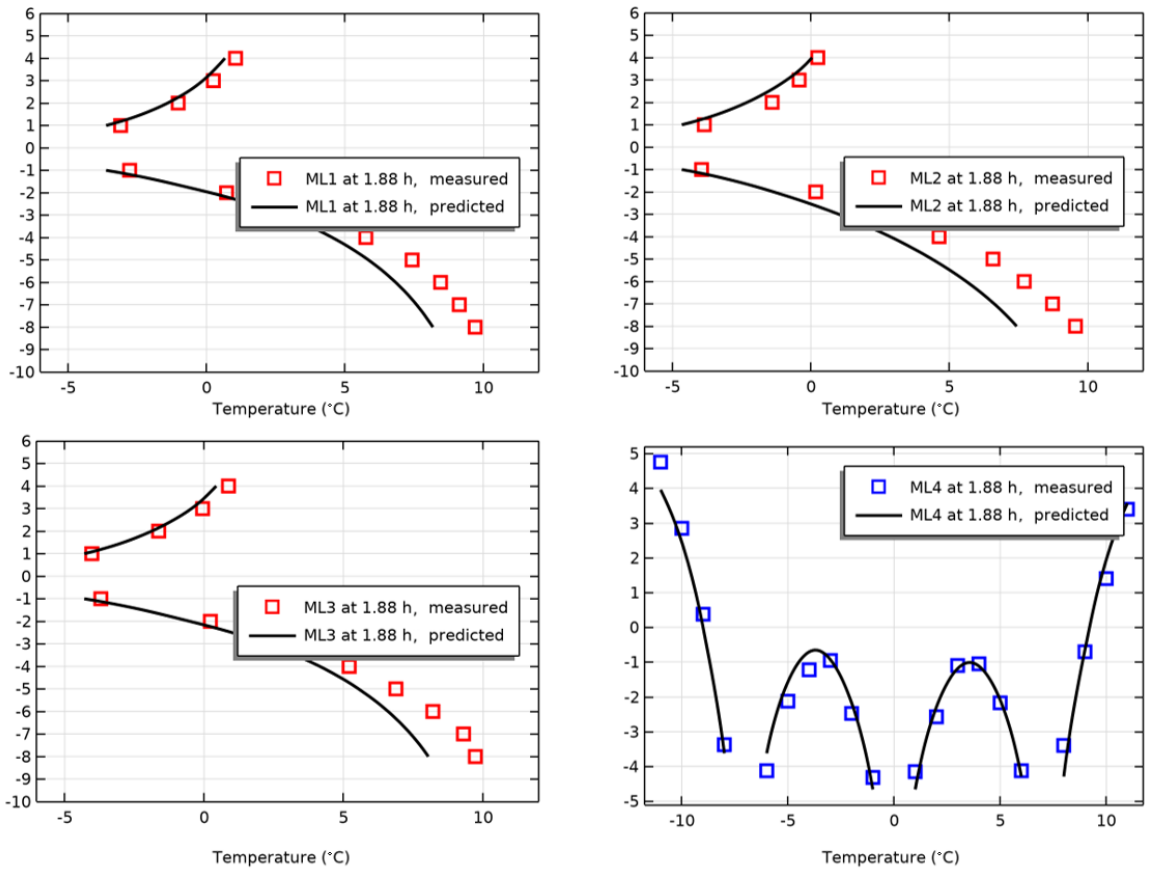

Fig. 10 Comparison of numerical and experimental results for i = 0.293

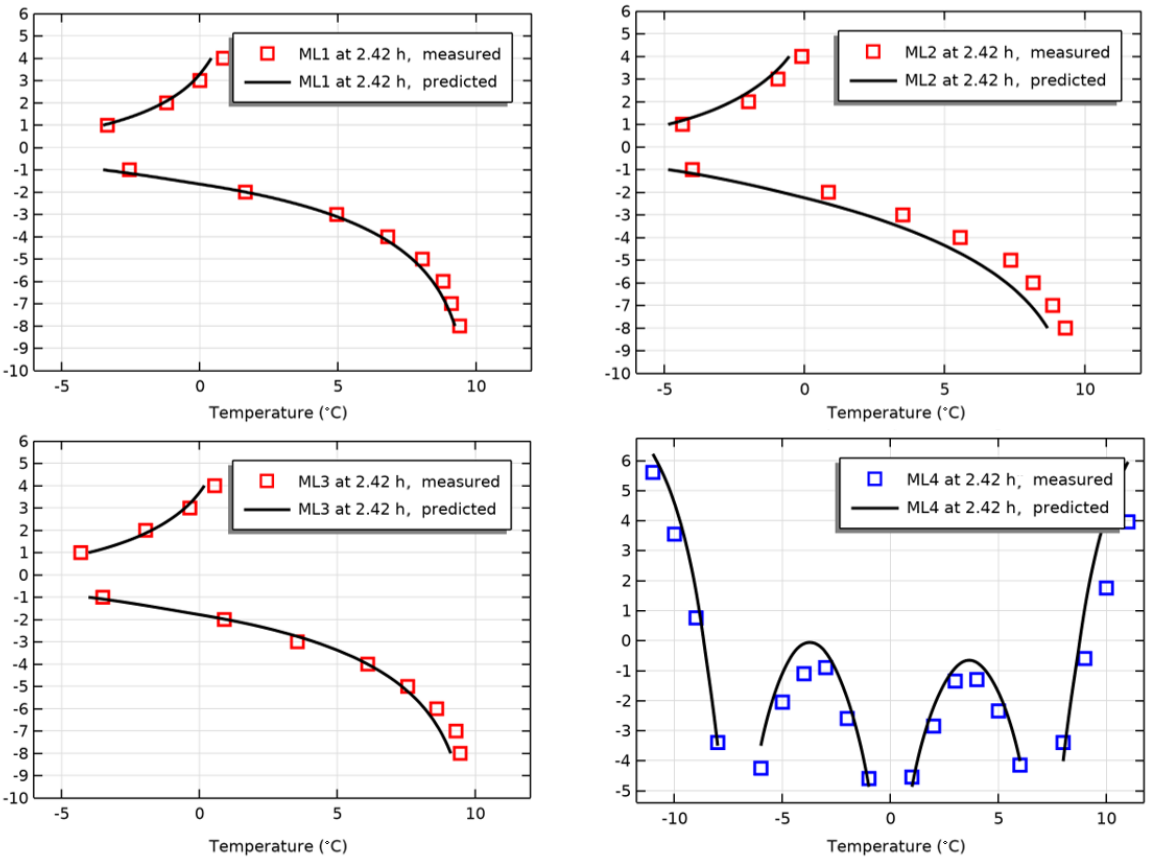

Fig. 11 Comparison of numerical and experimental results for i = 0.560

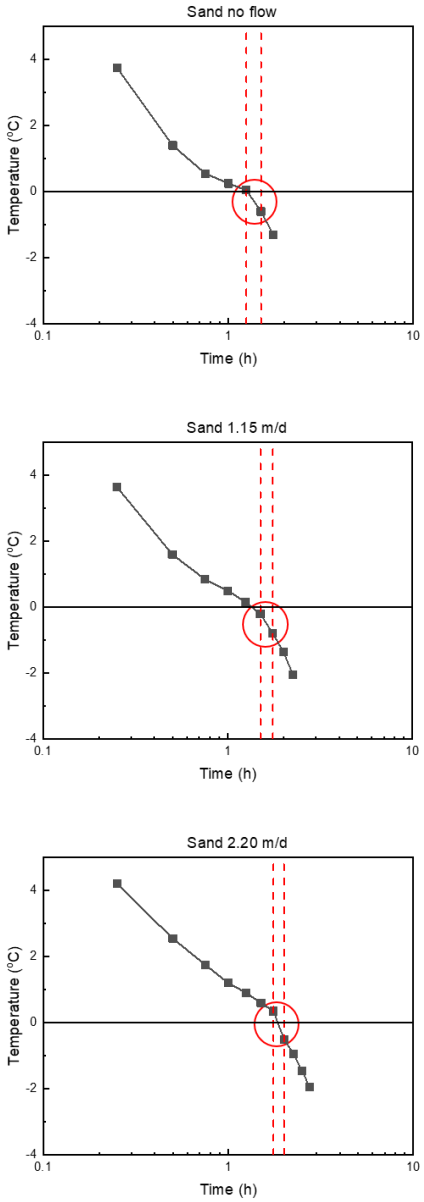

Fig. 12 T50 during freezing of saturated sandy soil

Table 4 Range of independent variables used in the parametric analysis

Parameter	Minimum	Maximum	Unit	Related to
Hydraulic gradient, i	0.3	0.9	-	Hydraulic behavior
Unfrozen permeability, k_{uf}	$0.5*k_{uf,ref}$	$2*k_{uf,ref}$	m^2	
Particle thermal conductivity, λ_s	2	6	$W\ m^{-1}\ K^{-1}$	Thermal behavior
Temperature at freeze pipes	−10	−5	℃	

$*k_{uf,ref} = 8.5 \times 10^{-12}\ m^2$ (Reference unfrozen permeability)

Fig. 15 summarizes the parametric study's results on the influencing factors. As λ_s increases, the closure time decreases; the change is more sensitive when the flow velocity is high. The effect of k_{uf} on the closure time was relatively small when λ_s is high: at high λ_s, the thermal conduction effect by λ_s dominates that of the groundwater

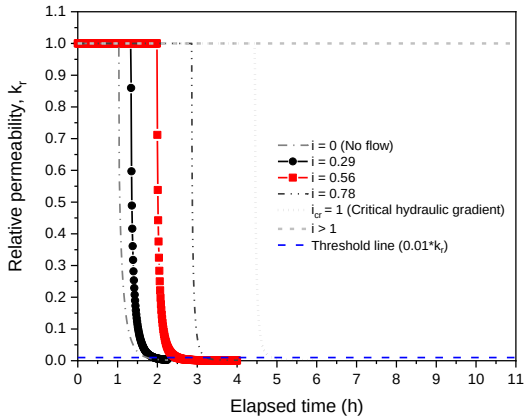

Fig. 13 Relative permeability with time at T50

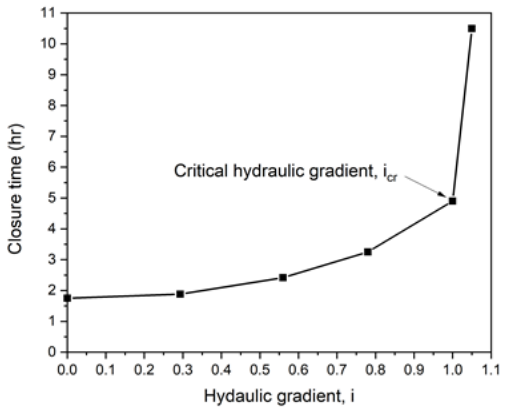

Fig. 14 Closure time variation with regard to the hydraulic gradient

flow; Fig. 15 also shows the effect of the temperature of the freeze pipes. Closure time is affected more sensitively by k_{uf} and λ_s when the cooling temperature is relatively high (−5℃) than when it is relatively low (−10℃). Overall, although the parameters related to the hydro-thermal behavior affect the closure time, the cooling temperature is the most dominant factor.

7. Conclusions

This study reports a new closed-loop AGF model with vertical flow and AGF tests conducted under various water flow conditions. After verifying the testing equipment, a method of estimating closure time using temperature measurements was reviewed in detail. A further parametric study of closure time—which determines the efficiency of the AGF technique—was conducted using a two-dimensional coupled thermal–hydraulic numerical model. The following conclusions were drawn.

- A closed-loop AGF laboratory testing system simulating vertical flow from bottom upward was newly developed for accurate calculation of groundwater flow

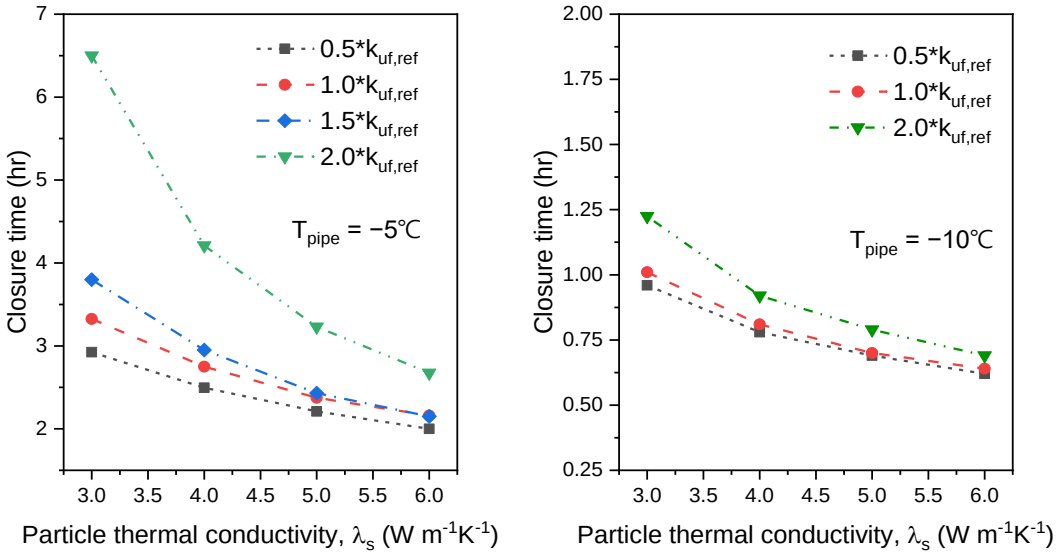

Fig. 15 Results of parametric study of influencing factors

velocity, which is the most important factor in AGF. The set up could record reliable experimental data through precise flow control. It is expected to be useful for experimental and numerical studies of AGF.

- Semi-logarithmic plots of temperatures measured between adjacent neighboring freeze pipes (T50) with respect to time showed inflection points at the closure time. As the frozen soil–ice wall formed, pore ice, which has a higher thermal conductivity than water, replaced the pore water; the temperature drops thus accelerated, leading to an inflection point in the data. Therefore, the closure time can be estimated indirectly using only temperature measurements between adjacent neighboring freeze pipes.
- A parametric study using a two-dimensional thermal–hydraulic coupled numerical analysis model examined factors affecting the closure time. Lower particle thermal conductivity, higher unfrozen soil permeability, and raising the freeze pipe temperature increase the closure time. Although all the considered parameters affected the system's freezing behavior, the formation of frozen soil–ice walls became less sensitive to changes in the unfrozen permeability and particle thermal conductivity if the cooling temperature of the freeze pipe was low enough.

Acknowledgments

This research was supported by the research project "Development of environmental simulator and advanced construction technologies over TRL6 extreme conditions" funded by the Korea Institute of Civil Engineering and Building Technology (KICT).

References

Alzoubi, M.A., Nie-Rouquette, A. and Sasmito, A.P. (2018). "Conjugate heat transfer in artificial ground freezing using enthalpy-porosity method: Experiments and model validation", *Int. J. Heat Mass Tran.*, **126**(A), 740-752. https://doi.org/10.1016/j.ijheatmasstransfer.2018.05.059.

Alzoubi, M.A., Madiseh, A., Hassani, F.P. and Sasmito, A.P. (2019), "Heat transfer analysis in artificial ground freezing under high seepage; Validation and heatlines visualization", *Int. J. Therm. Sci.*, **139**, 232-245. https://doi.org/10.1016/j.ijthermalsci.2019.02.005.

Alzoubi, M.A., Xu, M., Hassani, F.P., Poncet, S. and Sasmito, A.P. (2020), "Artificial ground freezing: A review of thermal and hydraulic aspects", *Tunn. Undergr. Sp. Tech.*, **104**, 103534-1-18. https://doi.org/10.1016/j.tust.2020.103534.

Andersland, O.B. and Ladanyi, B. (2004), *Frozen Ground Engineering* (2nd Edition), John and Wiley Sons, NY, USA.

Chang, M., Mao, T.W. and Huang, R.C. (2016), "A study on the improvements of geotechnical properties of in-situ soils by grouting", *Geomech. Eng.*, **10**(4), 527-546. http://dx.doi.org/10.12989/gae.2016.10.4.527.

Comsol Inc. (2021), *Comsol Multiphysics User's Manual Ver. 5.6*, Comsol Inc., Burlington, MA, USA.

Coussy O. (2004), *Poromechanics*, John and Wiley Sons, New York, NY, USA.

Frivik, P. and Comini, G. (1982), "Seepage and heat flow in soil freezing", *J. Heat Transf.*, **104**(2), 323-328. https://doi.org/10.1115/1.3245091.

Hashemi, H.T. and Sliepcevich, C.M. (1973), "Effect of seepage stream on artificial soil freezing", *J. Soil Mech. Found. Div.*, **99**(3), 267-289. https://doi.org/10.1061/JSFEAQ.0001861.

Go, G.H., Lee, J. and Kim, M. (2020), "Influencing factors on freezing characteristics of frost susceptible soil based on sensitivity analysis", *J. Korean Geotech. Soc*, **36**(8), 49-60. https://doi.org/10.7843/kgs.2020.36.8.49.

Huang, S., Guo, Y., Liu, Y., Ke, L., Liu, G. and Chen, C. (2018), "Study on the influence of water flow on temperature around freeze pipes and its distribution optimization during artificial ground freezing", *Appl. Therm. Eng.*, **135**, 435-445. https://doi.org/10.1016/j.applthermaleng.2018.02.090.

Jessberger, G.L. (1980), "Theory and application of ground freezing in civil engineering", *Cold Reg. Sci. Technol.*, **3**, 3-27. https://doi.org/10.1016/0165-232X(80)90003-8.

Jin, H., Lee, J., Ryu, B.H. and Go, G.H. (2020), "Experimental and numerical study on hydro-thermal behaviour of artificial

freezing system with water flow", *J. Korean Geotech. Soc.*, **36**(12), 17-25. https://doi.org/10.7843/kgs.2020.36.12.17.

Jumikis, A.R. (1979), "Cryogenic texture and strength aspects of artificially frozen soils", *Eng. Geol.*, **13**, 125-135. https://doi.org/10.1016/0013-7952(79)90026-7.

Lackner, R., Amon, A. and Lagger, H. (2005), "Artificial ground freezing of fully saturated soil: Thermal problem", *J. Eng. Mech.*, **131**(2), 211-220. https://doi.org/10.1061/(ASCE)0733-9399(2005)131:2(211).

Li, Z., Chen, J., Sugimoto, M. and Ge, H. (2019), "Numerical simulation model of artificial ground freezing for tunneling under seepage flow conditions", *Tunn. Undergr. Sp. Tech.*, **92**, 103035. https://doi.org/10.1016/j.tust.2019.103035.

Luckner L., van Genuchten M.T. and Nielsen D.R. (1989), "A consistent set of parametric models for the two-phase flow of immiscible fluids in the subsurface", *Water Resour. Res.*, **25**(10), 2187-2193. https://doi.org/10.1029/WR025i010p02187.

Marwan, A., Zhou, M.M., Abdelrehim, M.Z. and Meschke, G. (2016), "Optimization of artificial ground freezing in tunneling in the presence of seepage flow", *Comput. Geotech.*, **75**, 112-125. https://doi.org/10.1016/j.compgeo.2016.01.004.

Michalowski, R.L. and Zhe, M. (2006), "Frost heave modelling using porosity rate function", *Int. J. Numer. Anal. Meth. Geomech.*, **30**, 703-722. https://doi.org/10.1002/nag.497.

Pimentel, E., Papakonstantinou, S. and Anagnostou, G. (2012a), "Numerical interpretation of temperature distributions from three ground freezing applications in urban tunnelling", *Tunn. Undergr. Sp. Tech.*, **28**, 57-59. https://doi.org/10.1016/j.tust.2011.09.005.

Pimentel, E., Sres, A. and Anagnostou, G. (2012b), "Large-scale laboratory tests on artificial ground freezing under seepage-flow conditions", *Géotechnique*, **62**(3), 227-241. https://doi.org/10.1680/geot.9.P.120.

Quang, N.D. and Giao, P.H. (2014), "Improvement of soft clay at a site in the Mekong Delta by vacuum preloading", *Geomech. Eng.*, **6**(5), 419-436. http://dx.doi.org/10.12989/gae.2014.6.5.419.

Shen, Y., Wang, Y., Zhao, X., Yang, G., Jia, H. and Rong, T. (2018), "The influence of temperature and moisture content on sandstone thermal conductivity from a case using the artificial ground freezing (AGF) method", *Cold Reg. Sci. Technol.*, **155**, 149-160. https://doi.org/10.1016/j.coldregions.2018.08.004.

Shin, H., Kim. J. and Lee, J. (2018), "Effect of groundwater flow on ice-wall integrity", *J. Korean Geotech. Soc.*, **34**(11), 43-55. https://doi.org/10.7843/kgs.2018.34.11.43.

Ständer, W. (1967) *Mathematische Ansätze zur Berechnung der Frostausbreitung in ruhendem Grundwasser im Vergleich zu Modelluntersuchungen für verschiedene Gefrierrohranordnungen im Schactund Grundbau,* Technical University Fridericiana, Institute for Soil Mechanics and Rock Mechanics, Karlsruhe, Germany.

Taha, M.R., Alsharef, J.M.A., Khan, T.A., Aziz, M. and Gaber, M. (2018), "Compressive and tensile strength enhancement of soft soils using nanocarbons", *Geomech. Eng.*, **16**(5), 559-567. https://doi.org/10.12989/gae.2018.16.5.559.

Takashi, T. (1969), "Influence of seepage stream on the joining of frozen zones in artificial soil freezing", *Proceedings of International Conference on Effects of Temperature and Heat on Engineering Behavior of Soils,* Washington, January.

Tandel, Y.K., Solanki, C.H. and Desai, A.K. (2014), "Field behaviour geotextile reinforced sand column", *Geomech. Eng.*, **6**(2), 195-211. http://dx.doi.org/10.12989/gae.2014.6.2.195.

Vitel, M., Rouabhi, A., Tijani, M. and Guerin, F. (2016), "Modeling heat and mass transfer during ground freezing subjected to high seepage velocities", *Comput. Geotech.*, **73**, 1-15. https://doi.org/10.1016/j.compgeo.2015.11.014.

Wang, B., Rong, C.X., Lin, J., Cheng, H. and Cai, H.B. (2019), "Study on the formation law of the freezing temperature field of freezing shaft sinking under the action of large-flow-rate groundwater", *Adv. Mater. Sci. Eng.*, **2019**(1670820), 1-20. https://doi.org/10.1155/2019/1670820.

Yu, W.B., Liu, W.B., Lai, Y.M., Chen, L. and Yi. X. (2014), "Nonlinear analysis of coupled temperature-seepage problem of warm oil pipe in permafrost regions of Northeast China", *Appl. Therm. Eng.*, **70**, 988-995. https://doi.org/10.1016/j.applthermaleng.2014.06.028.

Zhou, M.M. and Meschke, G. (2013), "A three-phase thermo-hydro-mechanical finite element model for freezing soils", *Int. J. Numer. Anal. Meth. Geomech.*, **37**, 3173-3193. https://doi.org/10.1002/nag.2184.

Zhou, J. and Tand, Y. (2018), "Experimental inference on dual-porosity aggravation of soft clay after freeze-thaw by fractal and probability analysis", *Cold Reg. Sci. Technol.*, **153**, 181-196. https://doi.org/10.1016/j.coldregions.2018.06.001.

Zueter, A., Nie-Rouquette, A., Alzoubi, M.A. and Sasmito, A.P. (2020), "Thermal and hydraulic analysis of selective artificial ground freezing using air insulation: Experiment and modelling", *Comput. Geotech.*, **120**, 103416. https://doi.org/10.1016/j.compgeo.2019.103416.

IC